Molecular Weight Dependence of Polymersome Membrane Structure, Elasticity, and Stability

Harry Bermudez,[†] Aaron K. Brannan,[‡] Daniel A. Hammer,[†] Frank S. Bates,[‡] and Dennis E. Discher*[,†]

Department of Chemical and Biomolecular Engineering, University of Pennsylvania, Philadelphia, Pennsylvania 19104, and Department of Chemical Engineering and Materials Science, University of Minnesota, Minneapolis, Minnesota 55455

Received April 30, 2002; Revised Manuscript Received July 26, 2002

ABSTRACT: Vesicles prepared in water from a series of diblock copolymers—"polymersomes"—are physically characterized. With increasing molecular weight $\bar{M}_n$, the hydrophobic core thickness for self-assembled bilayers of poly(ethylene oxide)−polybutadiene increases up to ∼20 nm, which is considerably greater than any previously studied lipid or polymersome system. Micromanipulation of vesicles demonstrates an interface-dominated elasticity that is independent of $\bar{M}_n$. Furthermore, membrane stability as defined by the maximal areal strain increases with $\bar{M}_n$, approaching a universal limit predicted by mean-field ideas and set by the interfacial tension. Nonlinear responses and memory effects also emerge with increasing $\bar{M}_n$, indicating the onset of chain entanglements at higher $\bar{M}_n$. The results highlight the interfacial limits and transitions to bulk responses of self-assemblies.

Introduction

Biological systems have long been appreciated as exploiting aqueous self-assembly; synthetic amphiphiles of many types have also been shown to spontaneously self-assemble into highly ordered structures in water.[1−7] Depending on temperature and molecular characteristics, numerous morphologies are now possible, including vesicles, micelles, and more exotic structures. Even so, the factors contributing to microphase stability are not always clear at the nanoscale, where interfacial effects often dominate bulk interactions. Little more than interfaces that their membranes define, lipid vesicles or "liposomes"[8] are often considered prototypical from both a materials science and biological perspective.[9] However, practical applications involving liposomes have been continually hindered by a lack of stability.[10] Presumably commensurate with limits on membrane stability is the narrow range (3−5 nm) of the hydrophobic core thickness d of liposome membranes.[11] We extend here the range of d and explore the impact on membrane properties such as stability by forming vesicles from diblock copolymers of poly(ethylene oxide)−polybutadiene (PEO−PBD).[12]

Experimental Section

Materials. As listed in Table 1, a molecular weight series of PEO−PBD as well as PEO−poly(ethylethylene) was synthesized by standard living anionic polymermization techniques.[13] The number of monomer units in each block was determined by ^{1}H NMR. Gel permeation chromatography with polystyrene standards was used to determine number-average molecular weights $\bar{M}_n$as well as polydispersity indices (always <1.10). The PEO volume fraction is denoted by f_{EO}.

Preparation of Polymer Vesicles. Giant vesicles were made by standard film rehydration techniques.[14] Briefly, copolymer in chloroform solution was uniformly coated on the inside wall of a glass vial, followed by evaporation of the chloroform under vacuum. Addition of sucrose solution (250−300 mM), to give a final polymer concentration of 0.01 wt %, led to spontaneous formation of vesicles. Copolymers of higher molecular weight (i.e., **OB18**, **OB19**) required incubation at ∼60 °C to increase vesicle size and yield.

Table 1. Details of Vesicle-Forming Diblock Copolymers

designated name	polymer formula	$\bar{M}_n$ (kg/mol)	f_{EO}	d (nm)
OE7	EO_{40}-EE_{37}	3.9	0.39	8.0
OB2	EO_{26}-BD_{46}	3.6	0.28	9.6
OB16	EO_{50}-BD_{55}	5.2	0.37	10.6
OB18	EO_{80}-BD_{125}	10.4	0.29	14.8
OB19	EO_{150}-BD_{250}	20.0	0.28	21.0

Cryogenic Transmission Electron Microscopy (Cryo-TEM). Thin films (about 10−300 nm) of 1.0 wt % polymer in water were suspended in a microperforated grid. Samples were prepared in an isolated chamber with temperature and humidity control. The sample assembly was rapidly vitrified with liquid ethane at its melting temperature (∼90 K) and kept under liquid nitrogen until it was loaded onto a cryogenic sample holder (Gatan 626). Images (Figure 1) were obtained with a JEOL 1210 at 120 kV using a nominal underfocus of 6 μm for improved phase contrast and digital recording. More detailed descriptions and related examples can be found elsewhere.[15,16]

Optical Microscopy and Micromanipulation. A Nikon TE-300 inverted microscope was used with either bright-field illumination or phase contrast imaging. The latter was used when a difference in refractive indices was established between the interior and exterior solutions (e.g., sucrose inside and glucose outside). The contrast is visibly moderated by any exchange of solutes across the membrane. Narishige manipulators were connected to a custom manometer system with pressure transducers (Validyne, Northridge, CA) for control and monitoring of the aspiration pressure.

The micromanipulation technique[17,18] involves a giant vesicle being aspirated into a micropipet. From vesicle geometry, the applied pressure, and the aspirated projection length, one can calculate the imposed membrane tension τ, and the relative area dilation $\alpha \equiv \Delta A/A_0$.

Results and Discussion

Among all of the various vesicle-forming amphiphiles, including lipids, a key unifying feature is a hydrophilic fraction $f \approx 0.3-0.4$ (Table 1). Aqueous self-assembly

[†] University of Pennsylvania.
[‡] University of Minnesota.

10.1021/ma020669l CCC: $22.00
Published on Web 09/04/2002

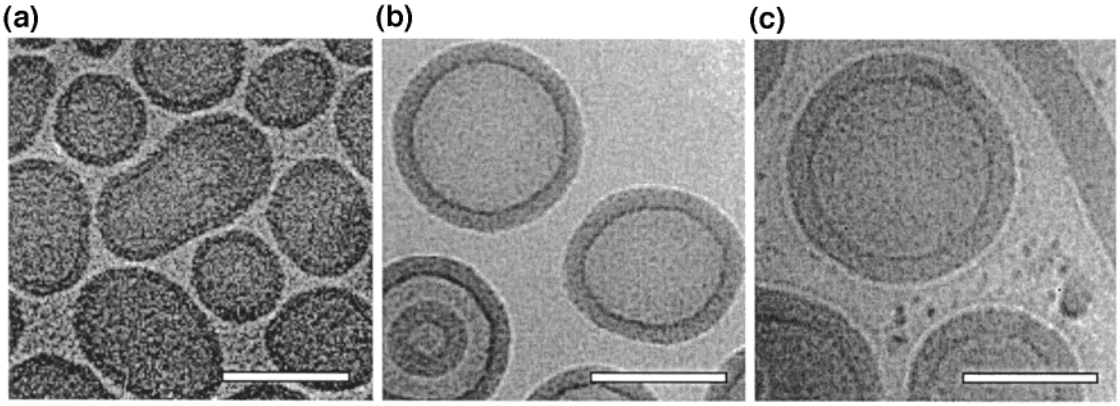

Figure 1. Cryo-TEM images of a 1.0 wt % aqueous solution of copolymer in water: (a) **OB2**, (b) **OB18**, and (c) **OB19**. The hydrophobic cores of polybutadiene are the darker areas. Scale bars are 100 nm. Polymorphism is common in cryo-TEM preparations but does not pose any difficulties to analysis since vesicles can be clearly identified from their concentric-ring structure.

of the present diblocks into membranes requires such proportions, as it is well-documented theoretically[19,20] and experimentally[21] that a larger f leads to wormlike and spherical micelles while smaller values of f yield inverted phases. Another shared feature of lipid membranes is their narrow range of hydrophobic core thickness d. Thus, connections between molecular conformations and mass, as well as the interplay between these factors in determining and limiting membrane self-assembly, have not been thoroughly studied. Direct imaging of our vesicles by cryo-TEM demonstrates a systematic increase in d with $\bar{M}_n$ (Table 1 and Figure 1).

It is important to note that the depth of field for cryo-TEM is comparable to the sample film thickness used. As such, the resulting image is effectively the projection of a sample's density into a plane. Assuming a membrane core of homogeneous density and spherical vesicles, the projected density has a maximum in the intensity I at the vesicle inner radius $r = R_i$. At $r = R_i + d$, the intensity will go to zero or, in our case, to the background intensity I_0. This simple model for the intensity is shown in Figure 2a, where d/R_i is used as a free parameter. For $d/R_i < 0.25$, the model is in excellent agreement with the measured profile (circumferentially averaged). The dark and light rings seen in Figure 1 are Fresnel interference fringes corresponding to the abrupt changes in the projected density at the inner and outer edges of the membrane, respectively. The fringes can also be seen in Figure 2a at $r = R_i$ and $r = R_i + d$, thus providing a simple means for determining the membrane thickness d. Similar analysis of spherical micelles via cryo-TEM gives very comparable results to corresponding SANS measurements.[12,21] Based on either fitting experimental profiles or edge detection (Figure 2b), measures of d seem to be independent of vesicle radius even though contrast is reduced for smaller vesicles.

Glassy diblock copolymers of PEO−polystyrene and poly(acrylic acid)−polystyrene have previously been shown to generate vesicular shells in organic mixtures with added water.[22] Although the effects of chain length and solvent have been studied in terms of morphological effects,[20,22] no clear trend between copolymer molecular weight and membrane thickness has yet been established. The thickness measurements here for our self-assembling copolymers suggest a scaling relationship between d and M_n. Noting that the mean hydrophobic molecular weight is given by $\bar{M}_h \sim \bar{M}_n(1 - f)$, the

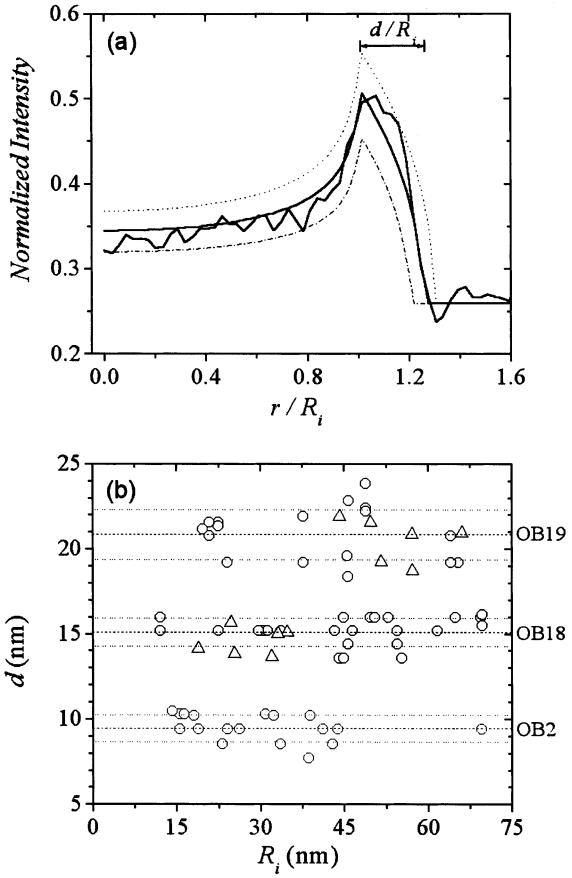

Figure 2. (a) Experimental intensity profile of a vesicle imaged by cryo-TEM. Best fit of the data corresponds to $d/R_i = 0.25$. Direct experimental estimation gives $d/R_i = 0.27$, which gives a difference of less than 1 nm. Dash−dot and dashed lines indicate fits using $d/R_i = 0.2$ and 0.3, respectively. Note the Fresnel interference fringe at $r/R_i \sim 1.3$. (b) Dependence of measured hydrophobic thickness d on inner radius R_i of vesicles imaged by cryo-TEM for **OB2**, **OB18**, and **OB19**. Solid and dashed lines are mean values ± S.D. Data are shown using spherical vesicles (○) and nonspherical vesicles (△) with out-of-plane curvature estimates.

experimental scaling of $d \sim (\bar{M}_h)^a$ leads to an exponent $a \sim 0.5$ (Figure 3). In theory, fully stretched chains would give $a = 1$ and ideal random coils would give $a = {}^1/_2$. Our copolymers are expected to be in the strong segregation limit (SSL), where a balance of interfacial tension and chain entropy yield a scaling of $a = {}^2/_3$.[19] The best-fit scaling exponent obtained surprisingly

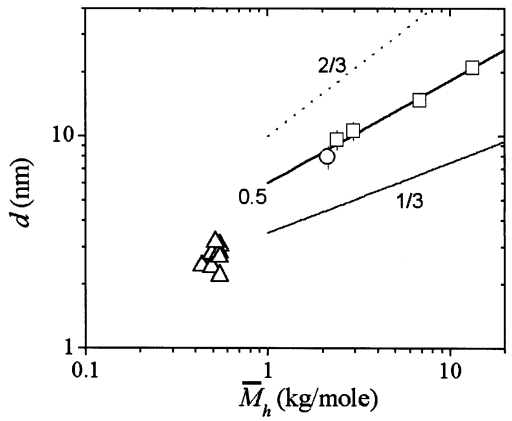

Figure 3. Scaling of the core thickness d with hydrophobic molecular weight $\bar{M}_h$. The best-fit scaling exponent of 0.5 is suggestive of chains in their unperturbed state. Exponents of $^1/_3$ and $^2/_3$ (solid gray and dashed gray, respectively) do not fit the data well. Data are shown for membranes of various phospholipids (△),[11] **OE7** (○), and the **OB** series (□).

suggests that chains in the various polymersome membrane cores are relatively unperturbed from their ideal state.

While lateral diffusivity decreases strongly with $\bar{M}_n$ for these polymers, **OE7** and **OB18** membranes have been clearly shown to be fluid via in-plane mobility measurements.[23] It is fluidity that generally allows for an equilibration of net forces underlying the scaling exponent a above. Furthermore, there is evidence for partial collapse of the PEO chains toward the interface, thus shielding the hydrophobic core from water.[21] This collapse would have the effect of increasing the equilibrium area per chain $\tilde{A}$ and thereby decreasing membrane thickness, consistent with the smaller exponent a compared to the SSL prediction (Figure 3). Assuming incompressibility, one can easily show that $\tilde{A} \sim (\bar{M}_h)^{0.5}$. Additional effects associated with relatively low-$\bar{M}_n$ polymers may also play a role in the unexpected scaling behavior.

Determinations of membrane elasticity and strength lend deeper insight into the interfacial and bulk forces at work within polymersome membranes. These forces have been probed by micropipet aspiration techniques (Figure 4) pioneered by Evans and co-workers with giant unilamellar lipid vesicles.[17] Plots of the effective membrane tension τ against the mean dilational strain α reveal an initial linear response as well as subsequent nonlinear and hysteretic effects. The latter are obvious for the thicker membranes **OB18** and **OB19** at areal strains (≈15−20%) much greater than those sustainable by any lipid membrane. Nevertheless, the reproducible initial slope of τ vs α defines an area elastic modulus K_a for the membrane (Figure 4).

Only one series of single-component phospholipid membranes (consisting of saturated and unsaturated phosphatidylcholines) has been thoroughly characterized. The most recent and refined measurements give $K_a \sim 240$ pN/nm.[18] The considerable thermal undulations of lipid membranes complicate K_a measurements, requiring a significant correction to account for the entropic contributions to area dilation. For our polymersomes this effect is mitigated by membranes that are substantially thicker and hence stiffer out-of-plane; thus, for **OE7** the correction to α is only about 1%.

In addition to hydrophobic interactions, other factors affecting K_a can arise from the counterion pairing

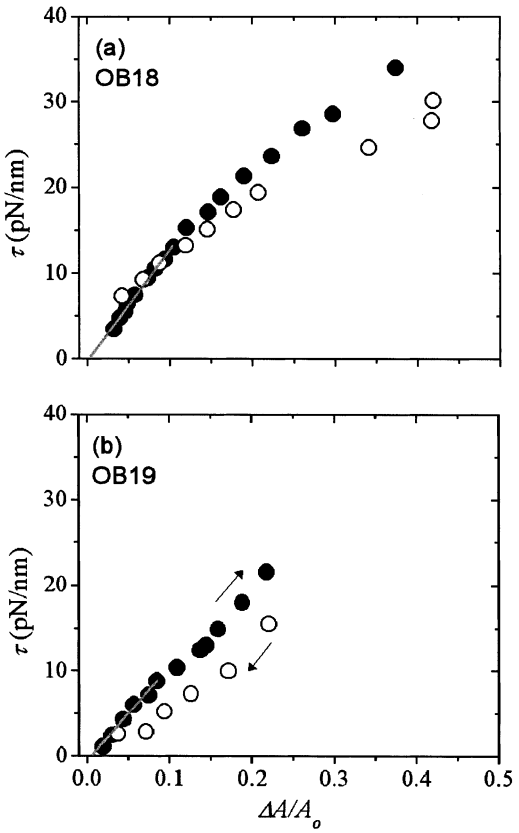

Figure 4. Determination of mechanical properties by micropipet aspiration. The applied tension t is plotted against areal strain $\alpha \equiv \Delta A/A_0$ and the area elastic modulus K_a is determined from the initial slope. Unlike **OE7** vesicles whose aspiration is entirely reversible,[6] hysteresis is observed after large strains imposed upon **OB18** and **OB19** vesicles. (a) **OB18** vesicle aspiration (●) and subsequent release (○). (b) **OB19** aspiration. In all experiments the loading rate ranged from $\sim 1 \times 10^{-4}$ to 10×10^{-4} N m^{-1} s^{-1}, without a significant effect on the reported properties. Scale bar is 5 μm.

expected among zwitterionic amphiphiles or the presence of small molecules, such as cholesterol, in the membrane. These complexities are avoided by the use of single-component neutral systems such as those here. Hence, we can essentially view K_a as being primarily related to the interfacial tension γ that reflects the chemical composition at each interface of the membrane. A simple area elasticity calculation[24] based on balancing molecular compression ($\sim 1/\tilde{A}$) against interfacial energy ($\sim \tilde{A}\gamma$) gives $K_a = 4\gamma$.

The chemical (rather than physical) basis for γ leads one to expect that K_a is independent of $\bar{M}_n$ (and hence d). Indeed, a mean K_a of 102 ± 10 pN/nm is obtained for all of the various polymersomes (Figure 5). The surface elasticity of the membrane thus depends *only* on the interface. Moreover, enthalpic interactions between PEO chains, which have been speculated to include H_2O bridging[25] or crystallization,[13] are either independent of PEO length or simply not a factor. A value of $\gamma = K_a/4 = 26$ pN/nm is also typical of oil−water interfaces. As mentioned, γ and χ are related and provide a measure of segregation between blocks; specifically, $\gamma \sim \sqrt{\chi}$.[26] The results thus suggest that a combined knowledge of amphiphile geometry (i.e., f) and interaction energies (χ) lead to predictive insights into membrane structure and elasticity.

While phosphatidylcholine membranes have a higher K_a than the present polymersome membranes, no lipid

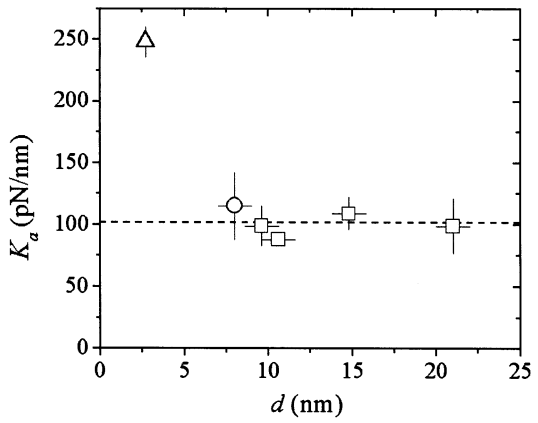

Figure 5. Molecular weight independence of the area elastic modulus K_a. The dominant factor in determining K_a is the interfacial tension γ, or equivalently, the interaction parameter χ that drives segregation. The membrane elasticity is thus determined strictly by the chemical composition of the interface and not the size of the molecule. Membranes of phosphatidylcholines (PC) have somewhat higher values of K_a,[18] reflecting the distinct composition. Data are shown for various PC (△), **OE7** (○), and **OB** (□) vesicles. Mean K_a is 102 ± 10 pN/nm.

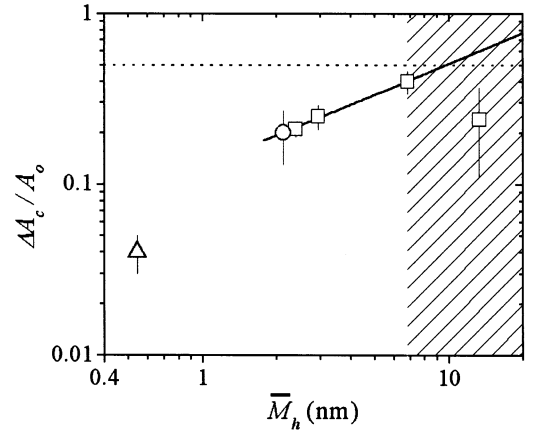

Figure 6. Areal strain at rupture $\alpha_c \equiv \Delta A_c/A_0$ vs hydrophobic molecular weight M_h. Scaling behavior with a power-law exponent ~0.6. Data are shown for SOPC (△), **OE7** (○), and **OB** (□) vesicles. The predicted upper limit of 50% is universal to bilayer systems. Note that lipid membranes are well below this bound and typically do not exceed ~5% areal strains. The hatched region schematically illustrates the molecular weight range where chain entanglements are thought to contribute.[27]

membrane can withstand a critical strain $\Delta A_c/A_0 \equiv \alpha_c$ of more than 5% before rupture, regardless of cholesterol addition. In contrast, the present synthetic systems can be strained to almost 50%; this depends on molecular weight as $\alpha_c \sim (\bar{M}_h)^{0.6}$ (Figure 6). At such large strains, an incompressible membrane will thin considerably to a reduced thickness $d_c \equiv d/(1 + \alpha_c)$. Using the previous relation $d \sim (\bar{M}_h)^a$ gives the scaling $\alpha_c \sim (d_c)^b$ with $b \sim 1.6$. Either scaling excludes the largest copolymer, **OB19**, which generally exhibits the earliest onset of hysteresis and falls well below the trend (Figure 6). As explained below, the apparent τ_c and α_c are both smaller for **OB19** ($\tau_c = 22 \pm 5$ pN/nm) than for **OB18** ($\tau_c = 33 \pm 5$ pN/nm). Thus, although larger copolymers allow for larger areas per chain $\bar{A}$, there are upper bounds on the stress and strain that can be sustained by a membrane.

The same balance of forces used to understand the SSL and membrane elasticity provides insight into membrane stability limits. The net chain pressure Π (core plus headgroup) and applied tension τ are balanced by the interfacial tension γ:

$$\Pi + \tau = 2\gamma \tag{1}$$

To account for the nonlinearity in the aspiration plots of Figure 4, the isotropic membrane tension is expanded to second order:

$$\tau(\alpha) = \tau_0 + K_a\alpha + \frac{1}{2}\frac{\partial^3 F}{\partial \alpha^3}\alpha^2 \tag{2}$$

Because of isotonic conditions, $\tau_0 = 0$. The experiments prove to be (e.g. Figure 4a) well-fit by

$$\tau(\alpha) = \tau_0 + K_a(\alpha - c\alpha^2) \tag{3}$$

with the coefficient $c \equiv -K_a^{-1}(^1/_2\partial^3 F/\partial\alpha^3)$ having the average value of 1.0 ± 0.2 for **OB16**, **OB18**, and **OB19**. Using the previously cited mean-field result of $K_a = 4\gamma$, we obtain

$$\Pi + K_a(\alpha - \alpha^2) = \frac{1}{2}K_a \tag{4}$$

and solve for α to arrive at

$$\alpha = \frac{1}{2}(1 \pm \sqrt{\Pi/\gamma - 1}) \tag{5}$$

From eq 5, there can only be real solutions provided that $\Pi \geq \gamma$. Noting that $\Pi = 2\gamma$ at zero applied tension, $\gamma \leq \Pi \leq 2\gamma$. Establishing the bounds for Π allows us to do the same for τ via eq 1 such that $\gamma \geq \tau \geq 0$. The upper bound for τ could also have been obtained by setting $d\tau/d\alpha = 0$ from eq 3.

By definition, $\alpha \geq 0$, but solutions of eq 5 with the positive root give $^1/_2 \leq \alpha \leq 1$ whereas those with the negative root give $0 \leq \alpha \leq {}^1/_2$. Only the latter makes physical sense, corresponding to $\Pi/\gamma \in [1,2]$ and $\tau/\gamma \in [1,0]$. The above bounds of $\alpha \leq {}^1/_2$ and $\tau \leq \gamma$ largely agree with the experimentally observed limits of polymersome membranes here. A related case where the membrane core is treated as a three-dimensional brush[18] leads to $K_a = 6\gamma$ and would give $\alpha \leq 0.21$, which is exceeded by polymersomes. As already noted, lipid membranes cannot withstand areal strains exceeding ≈5%, and therefore a strictly linear elastic response is not surprising. For such systems, the corresponding first-order analysis ($c = 0$) of the stabililty limit again yields $\alpha < {}^1/_2$ (independent of γ), although the additional conditions of $\Pi/\gamma \geq 1$ and $\tau/\gamma \leq 1$ would not be apparent.

The overall membrane behavior also appears rather insensitive to any local variations associated with finite polydispersity and seems instead dominated by the collective behavior of a fluid or meltlike state. Thus, the increased thickness (i.e., larger $\bar{M}_n$) makes the interface more readily self-healing. In natural membranes, by comparison, stiffening and toughening of the membrane are mediated by the small molecule cholesterol—presumably through cohesive healing of defects. However, the additional stability imparted by cholesterol to biomembranes cannot compare with that of a much thicker membrane. Thus, results here therefore imply that biomembranes are not designed for maximal stability but are instead optimized for a tenuous balance between stability and fluidity.

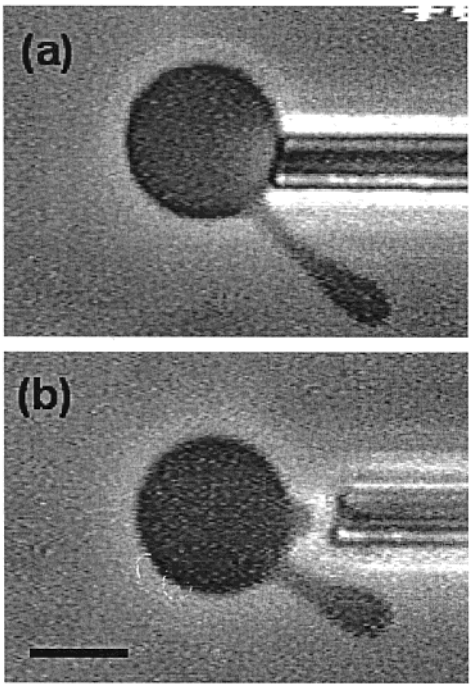

Figure 7. OB19 membranes do not relax quickly to their original state. The slow dynamics are apparent by initially aspirating an **OB19** vesicle to produce a long projection. (a) The vesicle is then released and reaspirated at a different location. (b) With increasing pressure, a second projection can be created before the first can completely relax. The vesicle is imaged under phase contrast, and the scale bar is 5 μm.

The basis for the strain softening seen here is not clear. The nonlinearity is not strongly dependent on deformation rate in the region tested ($(1-10) \times 10^{-4}$ N m^{-1} s^{-1}), suggesting that this is not a collective process involving many molecules but is instead a thermodynamic rearrangement at the molecular scale. We speculate that area dilation decreases PEO stretching and allows more collapse and hence shielding of the hydrophobic core. The proposed process is inspired in part by compressed monolayers which tend to show a decreased slope in their pressure isotherms during large dilations.

The decreased stability of the thickest membrane (**OB19**) is also unclear at this point but seems likely to be the result of increasing physical entanglements between chains. Figure 7 is representative of the very slow relaxation dynamics of **OB19** membranes. Even in **OB18**, membrane dynamics following electroporation are more than 100 times slower than **OE7** dynamics.[28] Furthermore, lateral diffusion coefficients beginning with **OB18** exhibit activated reptation,[23] which is a much stronger function of M_n than simple Rouse diffusion.

Provided that the time scale for aspiration is much smaller than the time scale for rearrangement among polymer chains (as is likely at the largest $\bar{M}_n$), the entanglements could act in a similar way to covalent cross-links. Surprising perhaps, but consistent with the results here, polymersome membranes with very low cross-link densities have been found to be weaker than un-cross-linked membranes.[29] This destabilization presumably arises through stress localization; that is, the tension τ is inhomogeneous over the membrane due to slow relaxations that oppose equilibration of forces.

Nonequilibrium effects indicated above can also be seen in $\tau-\alpha$ hysteresis loops following graded release from aspiration (Figure 4). Even down to low apparent areal strains of less than 10%, **OB19** exhibits marked hysteresis, whereas **OB18** aspiration appears reversible up to more modest strains of ~10−15%. In contrast, aspiration of **OE7** is reversible for nearly all strains up to lysis,[6] consistent with diffusion studies indicating Rouse-type mobility.[23] Hence, the hysteretic behavior in thicker membranes likely reflects relaxation times that scale strongly[31] with $\bar{M}_n$.

Conclusions

Vesicles formed by superamphiphiles provide new perspectives on some of the basic properties of bilayer membranes. By use of synthetic diblock copolymers, limitations of previous membrane systems have been considerably exceeded, providing novel insights into structure, scaling, and physical limits on lamellae. Specifically, the surface elasticity is found to be scale-independent, in accordance with simple mean-field theories. The membrane lysis tension τ_c and critical areal strain α_c are found to increase with $\bar{M}_n$, but only up to a simple limit. The onset of chain entanglements with higher $\bar{M}_n$ introduces bulk effects that eventually undermine interfacial elasticity through slowed response times. Examination of membranes assembled from PEO−PBD−PEO triblocks, where linear and looped configurations are expected, may help clarify such mechanisms. Of additional interest will be determinations of other properties such as the bending modulus which is expected to scale as $\sim K_a d^2$ for interface-dominated membranes.[9] Finally, while it is clear that lipid membranes found in nature are not maximally stable, it would seem they have developed sufficient stability while also providing the fluidity necessary for diverse functions.

Acknowledgment. This work was supported by NSF-MRSEC's at Penn and University of Minnesota as well as a materials science grant from NASA. H.B. thanks Dr. H. Aranda-Espinoza at Penn for many valuable conversations.

References and Notes

(1) Cornelissen, J. J. L. M.; Fischer, M.; Sommerdijk, N. A. J. M.; Nolte, R. J. M. *Science* **1998**, *280*, 1427.
(2) van Hest, J. C. M.; DeInoye, D. A. P.; Baars, M. W. P. L.; van Genderen, M. H. P.; Meijer, E. W. *Science* **1995**, *268*, 1592.
(3) Kramer, E.; Forster, S.; Goltner, C.; Antonietti, M. *Langmuir* **1998**, *14*, 2027.
(4) Nardin, C. Hirt; T.; Leukel, J.; Meier, W. *Langmuir* **2000**, *16*, 1035.
(5) Kaler, E. W.; Murthy, A. K.; Rodriguez, B. E.; Zasadzinski, J. A. N. *Science* **1989**, *245*, 1371.
(6) Discher, B. M.; Won, Y.-Y.; Ege, D. S.; Lee, J. C.-M.; Bates, F. S.; Discher, D. E.; Hammer, D. A. *Science* **1999**, *284*, 1143.
(7) Radzilowski, L. H.; Carragher, B. O.; Stupp, S. I. *Macromolecules* **1993**, *26*, 879.
(8) Bangham, A. D.; Standish, M. M.; Watkins, J. C. *J. Mol. Biol.* **1967**, *13*, 238.
(9) Lipowsky, R.; Sackmann, E. In *Structure and Dynamics of Membranes*; Elsevier: New York, 1995.
(10) Lasic, D. D.; Papahadjopoulos, D. In *Medical Applications of Liposomes*; Elsevier: New York, 1998.
(11) Marsh, D. *CRC Handbook of Lipid Bilayers*; CRC Press: Boca Raton, FL, 1990.
(12) Won, Y.-Y.; Davis, H. T.; Bates, F. S. *Science* **1999**, *283*, 960.
(13) Hillmyer, M. A.; Bates, F. S. *Macromolecules* **1996**, *29*, 6994.
(14) Menger, F. M.; Angelova, M. I. *Acc. Chem. Res.* **1998**, *31*, 789.
(15) Lin, Z.; He, M.; Scriven, L. E.; Davis, H. T. *J. Phys. Chem.* **1993**, *97*, 3571.

(16) Vinson, P. K.; Talmon, Y.; Walter, A. *Biophys. J.* **1989**, *56*, 669.
(17) Evans, E. A.; Skalak, R. *Mechanics and Thermodynamics of Biomembrane*s; CRC Press: Boca Raton, FL, 1980.
(18) Rawicz, W.; Olbrich, K. C.; McIntosh, T.; Needham, D.; Evans, E. *Biophys. J.* **2000**, *79*, 328.
(19) Bates, F. S.; Fredrickson, G. H. *Annu. Rev. Phys. Chem.* **1990**, *41*, 525. Bates, F. S. *Science* **1991**, *251*, 898.
(20) Szleifer, I.; Carignano, M. A. *Macromol. Rapid Commun.* **2000**, *21*, 423.
(21) Won, Y.-Y.; Davis, H. T.; Bates, F. S.; Agamalian, M.; Wignall, G. D. *J. Phys. Chem. B* **2000**, *104*, 7134.
(22) Yu, K.; Eisenberg, A. *Macromolecules* **1998**, *31*, 3509. Yu, Y.; Zhang, L.; Eisenberg, A. *Macromolecules* **1998**, *31*, 1144.
(23) Lee, J. C.-M.; Santore, M. M.; Bates, F. S.; Discher, D. E. *Macromolecules* **2002**, *35*, 323.
(24) Israelachvili, J. N. *Intermolecular and Surface Forces*; Academic Press: San Diego, CA, 1998.
(25) Naumann, C. A.; Brooks, C. F.; Fuller, G. G.; Lehmann, T.; Rhe, J.; Knoll, W.; Kuhn, P.; Nuyken, O.; Frank, C. W. *Langmuir* **2001**, *17*, 2801.
(26) Helfand, E.; Wasserman, Z. R. In *Developments in Block Copolymers*; Goodman, I., Ed.; Applied Science: New York, 1982; Vol. 1, p 99.
(27) Ferry, J. D. *Viscoelastic Properties of Polymers*; Wiley: New York, 1980.
(28) Aranda-Espinoza, H.; Bermudez, H.; Bates, F. S.; Discher, D. E. *Phys. Rev. Lett.* **2001**, *87*, 208301.
(29) Discher, B. M.; Bermudez, H.; Hammer, D. A.; Discher, D. E.; Won, Y.-Y.; Bates, F. S. *J. Phys. Chem. B* **2002**, *106*, 2848.
(30) Evans, E.; Ludwig, F. *J. Phys. (Paris)* **2000**, *12*, A315.
(31) Hamersky, M. W.; Hillmyer, M. A.; Tirrell, M.; Bates, F. S.; Lodge, T. P.; von Meerwall, E. D. *Macromolecules* **1998**, *31*, 5363.

MA020669L